LANGMUIR

Article

pubs.acs.org/Langmuir

Further Insight into the Definite Morphology and Formation Mechanism of Mesoporous Silica KCC-1

E. Febriyanti,[†] V. Suendo,*[,†,‡] R. R. Mukti,*[,†,‡] A. Prasetyo,[†] A. F. Arifin,[†] M. A. Akbar,[†] S. Triwahyono,[§] I. N. Marsih,[†] and Ismunandar[†]

[†]Division of Inorganic and Physical Chemistry, Faculty of Mathematics and Natural Sciences, and [‡]Research Center for Nanosciences and Nanotechnology, Institut Teknologi Bandung, Jl. Ganesha No. 10, Bandung 40132, Indonesia

[§]Department of Chemistry, Faculty of Science, Universiti Teknologi Malaysia, 81310 UTM Johor Bahru, Johor, Malaysia

Supporting Information

ABSTRACT: The unique three-dimensional pore structure of KCC-1 has attracted significant attention and has proven to be different compared to other conventional mesoporous silica such as the MCM-41 family, SBA-15, or even MSN nanoparticles. In this research, we carefully examine the morphology of KCC-1 to define more appropriate nomenclature. We also propose a formation mechanism of KCC-1 based on our experimental evidence. Herein, the KCC-1 morphology was interpreted mainly on the basis of compiling all observation and information taken from SEM and TEM images. Further analysis on TEM images was carried out. The gray value intensity profile was derived from TEM images in order to determine the specific pattern of this unique morphology that is found to be clearly different from that of other types of porous spherical-like morphologies. On the basis of these results, the KCC-1 morphology would be more appropriately reclassified as bicontinuous concentric lamellar morphology. Some physical characteristics such as the origin of emulsion, electrical conductivity, and the local structure of water molecules in the KCC-1 emulsion were disclosed to reveal the formation mechanism of KCC-1. The origin of the KCC-1 emulsion was characterized by the observation of the Tyndall effect, conductometry to determine the critical micelle concentration, and Raman spectroscopy. In addition, the morphological evolution study during KCC-1 synthesis completes the portrait of the formation of mesoporous silica KCC-1.

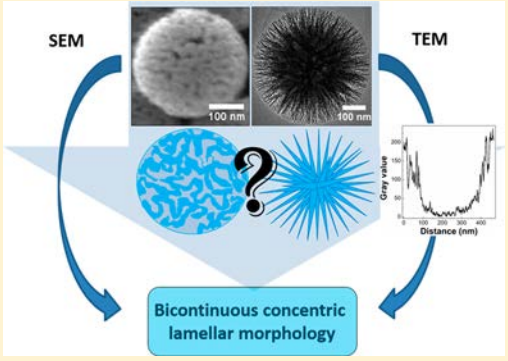

INTRODUCTION

The morphologically controlled synthesis of nanoporous materials brings about advancement and breakthroughs in a wide variety of applications, particularly in the area of catalysis as a support for catalytic active metals.[1,2] The synthesis technique has shown significant progress, resulting in nanoporous materials with a wide range of architectures.[3,4] Fine tuning the property of nanoporous materials can be done these days by appreciating the breakthrough of surfactant-templating synthesis discovered in the early 1990s that realizes the birth of a series of mesoporous materials.[5−8] Recently, unique mesoporous material with a high surface area such as KCC-1 was reported by Polshettiwar et al.[9,10] KCC-1 shows unique morphology that is responsible for the superior activity and stability when applied in certain catalytic reactions,[11−14] adsorption process,[15] and drug delivery.[16] Notably, the morphology and pore size are functional properties that need to be tailored.[17,18]

A morphological term is given to a particular nanomaterial on the basis of a morphological characteristic derived from scanning electron microscopy (SEM) and transmission electron microscopy (TEM) images. In the case of KCC-1, several terms have been used to describe its morphology such as fibrous,[9] nanoflowers,[19] radial wrinkle structure,[20] and dendritic structure.[21] Therefore, a specific terminology has yet to be assigned to describe the unique morphology of KCC-1. The different morphological terminologies used also indicate that the morphology of KCC-1 has not been fully revealed. This happened because the interpretation of KCC-1 is merely based on one type of microscopy observation from either SEM or TEM (Figure 1). The papers published thus far do not seem to combine both observations taken from SEM and TEM images.[9,19−21] A more representative definiton of KCC-1 morphology should beneficially give a better understanding in studying the formation mechanism.

The unprecedented morphology of KCC-1 has attracted much attention to the study of its formation mechanism. The mechanism is considered to be complex and remains unsolved. It is predicted that the formation of KCC-1 involves a water-in-oil (w/o) emulsion and reverse micelles. However, not all of the proposed mechanisms are experimentally tested, and some of them contradict principles of chemistry.[9,19,20]

Herein, we report a thorough study to revisit the nomenclature of KCC-1 morphology and its rational formation mechanism.

Received: February 25, 2016
Revised: April 21, 2016
Published: April 27, 2016

DOI: 10.1021/acs.langmuir.6b00675
Langmuir 2016, 32, 5802−5811

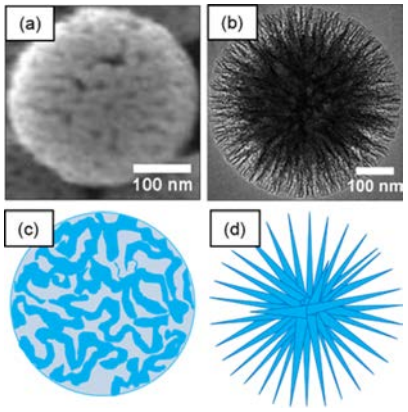

Figure 1. (a) SEM and (b) TEM images of KCC-1 with their respective illustration drawn in (c) and (d), respectively.

The KCC-1 morphology was interpreted after observing and analyzing SEM and TEM images. The TEM images were converted to gray value intensity patterns that were markedly different from other types of porous spherical-like morphologies. As for the formation mechanism, this article also explains the principal contribution of emulsion and the micelle state-of-art during the synthesis of KCC-1.

EXPERIMENTAL SECTION

Synthesis. Cetyltrimethylammonium bromide (CTAB) was purchased from Sigma-Aldrich. Tetraethyl orthosilicate (TEOS), urea, toluene, and *n*-butanol were puchased from Merck.

KCC-1 was synthesized by applying a solvothermal treatment. In a typical synthesis, *n*-butanol (0.73 mL) was dissolved in toluene (17.05 mL), followed by adding TEOS (1.55 mL). Subsequently, a solution of CTAB (0.55 g) and urea (0.35 g) in deionized water (17.30 mL) was quickly added the above solution. After vigorous stirring for 30 min, the mixture that turned into an emulsion (for further discussion this emulsion is refer to as a KCC-1 emulsion) was transferred to a 50 mL Teflon-lined autoclave and held at 120 °C for 4 h. The resulting product was isolated by centrifugation, washed with deionized water and acetone, and dried in air for 24 h. Finally, the as-synthesized product was calcined at 550 °C for 6 h in air. For the systematic study, we performed the synthesis of KCC-1 using the above synthesis procedure in various H_2O/Si (0.1−0.4) and CTAB/Si (50−200) molar ratios.

Characterization. The resulting KCC-1 was characterized with a nitrogen sorption Quantachrome autosorb iQ-MP instrument at 77 K in which the samples were pretreated at 300 °C for 3 h under ultrahigh vacuum. SEM images and TEM images of KCC-1 were obtained using JEOL-JSM-6510 LV and JEOL JEM 1400 microscopes, respectively. TEM images were then analyzed using ImageJ software. The XRD patterns were recorded on a Rigaku Ultima III diffractometer with Cu Kα (λ = 1.5406 Å) radiation.

Conductance of the KCC-1 precursor emulsion was measured to determine the critical micelle concentration (cmc). The cmc was evaluated from a plot of the specific conductance (κ) against surfactant concentration.[22] An emulsion containing CTAB/H_2O/toluene/*n*-butanol was analyzed by a Metler Toledo SevenEasy conductometer at 26.2 ± 0.5 °C. To prepare the emulsion, CTAB (0.018 g), H_2O (4.85 mL), toluene (4.8 mL), and *n*-butanol (0.2 mL) were mixed. A series of emulsions were prepared via a varying CTAB concentration in the range of 10−100 mM with an oil-to-water volume ratio equal to 1.03. The emulsion was also characterized by Raman spectroscopy. The experiment was carried out in flow-through mode to ensure that the emulsion was well mixed during measurement (Figure 2). The emulsion was prepared in a plastic beaker that was connected to a capillary glass tube Raman cell (2 mm outer diameter and 25 μm thick walls) via silicon tubing. The emulsion in the beaker was continuously

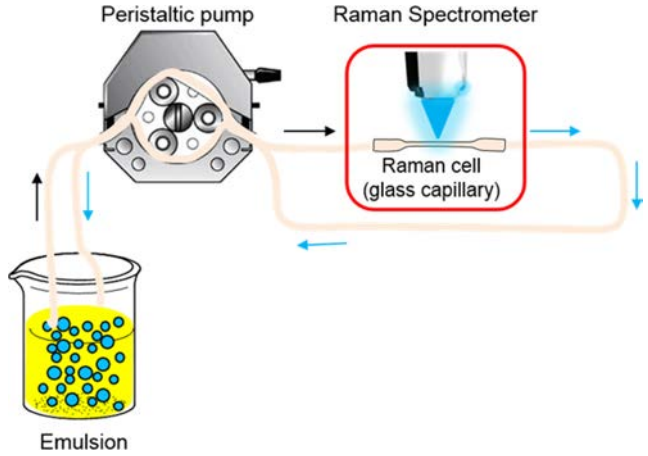

Figure 2. Schematic image of a continuous flow-through Raman spectroscopy experiment for studying an emulsion.

stirred and circulated via a peristaltic pump from the beaker through the glass capillary Raman cell and back into the beaker (Figure 2). The spectra were recorded on Senterra Raman spectrometer (Bruker Optics, Inc.) at room temperature using a diode laser at 488 nm with a power of 40 mW. The resolution of the Raman spectral recording was 2 cm^{-1}. Raman spectra were fitted with multiple Gaussian functions. As a comparison, Raman analysis was also carried out on a CTAB micellar solution (CTAB dissolved in water, ∼7 mM), toluene, and pure water.

RESULTS AND DISCUSSION

Revisiting the KCC-1 Morphology. The fact that there are several terms used to describe the KCC-1 morphology has motivated us to revisit and find reliable scientific facts by means of recharacterization, reanalysis, and reinterpretation of the KCC-1 morphology. One of the characterization methods to reveal the KCC-1 morphology pattern can be performed by quantitatively analyzing the TEM images. TEM images were converted into line profiles representing the gray value intensity[23,24] (Figure 3). The gray values were extracted along the preselected line across the TEM images.

The TEM image has different gray value intensities over different areas. A lower gray value intensity corresponds to darker area, whereas a lighter area has a higher gray value intensity. A plot of these intensities along a line crossing the image forms a characteristic pattern specific to a certain type morphology. For example, U-like and W-like plots correspond to dense (nonporous) and hollow-type material, respectively (Figure 3a,b). Material with a high degree of porosity such as spherical-like ordered mesoporous material has a wavy pattern (Figure 3c). Some materials may have similar TEM profile patterns. For instance, the multishell type material has a W-like pattern that is similar to that of a hollow-type material (Figure 3d). However, there are additional features in the outermost edge that could differentiate them. On the other hand, the egg-yolk-type material shows an inverse W-like pattern (Figure 3e).

Figure 3f,g shows the TEM profile pattern derived from a hollow-type hierarchical pore structure and core−shell type material, respectively. The W-like pattern of hollow type with hierarchical pore structure material has fine features in the center region. The presence of this fine feature can be understood from the small pores, wrinkles, sheets, or any stacked/folded/rolled lamella contained in the material. The core−shell-type material has a pattern similar to the U-like pattern except for the negative plateaus on the left and right parts. This core−shell-type material

DOI: 10.1021/acs.langmuir.6b00675
Langmuir 2016, 32, 5802−5811

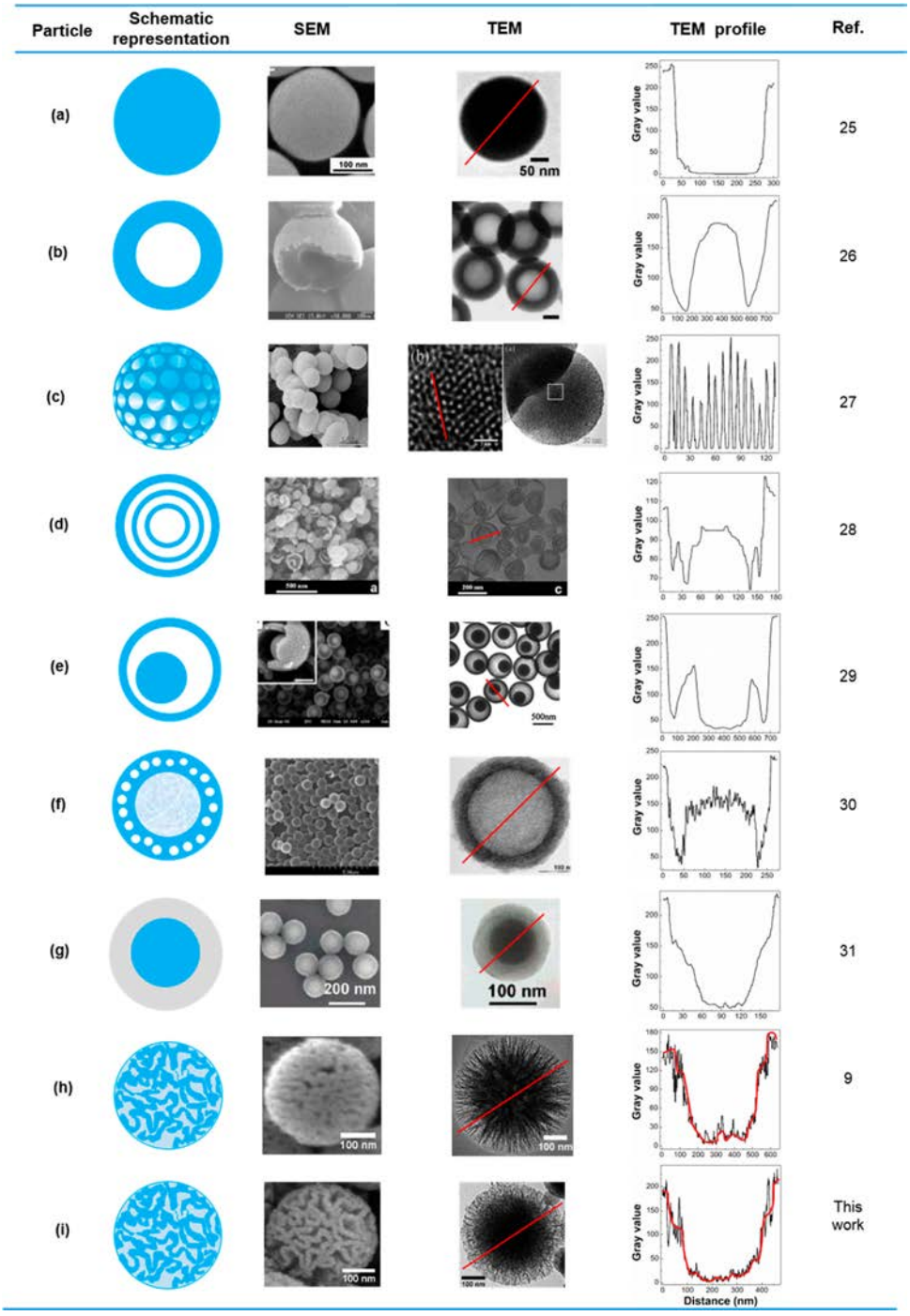

Figure 3. Silica particles in various morphologies were observed by SEM and TEM images. The morphology nomenclature for these particles is defined as (a) nonporous/dense,[25] (b) hollow,[26] (c) ordered mesoporous,[27] (d) multishell,[28] (e) core in hollow (rattle/egg yolk),[29] (f) hollow with hierarchical pores,[30] (g) core−shell,[31] (h) KCC-1,[9] and (i) reproduced KCC-1 (this work). The morphologies were redrawn in schematic illustrations, and the gray value intensity profiles for each morphology were derived by analyzing each TEM image. The red lines on TEM images are the working area resulting in the gray value intensity of the TEM profile. The red lines on TEM profiles of KCC-1 were drawn to simply show the profile pattern.

is characterized by concentric spherical morphology. This morphology has a denser core than the outer part (Figure 3). These two patterns are useful for identifying the KCC-1 morphology. As we look at the KCC-1 profile (Figure 3h), the pattern shows a shape similar to the core−shell-type material displaying negative plateaus on the right and left parts as well as shape similar to hollow type with hierarchical pore structure material displaying fine features throughout the particle.

It has been understood that the KCC-1 morphology has a combination of features of concentric and porous material as shown in the TEM profile. In the case of KCC-1, it is not necessary to intepret the fine feature as pores. The high surface area of KCC-1 can be attributed to the fine features in the shell and core in the form of wrinkles or lamellar structure and is not due to the presence of pores.[9,10,20] Thus, along with the SEM images, KCC-1 can be described to have a

DOI: 10.1021/acs.langmuir.6b00675
Langmuir 2016, 32, 5802−5811

spherical bicontinuous (top view)[11,20] and concentrically stacked lamellar shape (cross section).[15,20,32] In general, we would like to coin the KCC-1 morphology as bicontinuous concentric lamellar.

Our work reveals the reproducibility of KCC-1 in which the morphology and TEM profile are comparable to the previous reports (Figure 3i). KCC-1 materials have been successfully prepared, starting from reaction mixtures with different compositions. The variation of reaction mixture used is presented in Figure 4. The resulting products show typical bicontinuous lamellar morphology as characterized by SEM (Supporting Information, Figure S1 and S2). The X-ray diffractogram of KCC-1 shows two broadened peaks at 2θ of 1−5° and 15−37° that correspond to low and high diffraction angles, respectively. Normally, the appearance of this typical broadened peak at low angle is attributed to the presence of wormhole-type mesoporous material.[33] Further calculation using the Scherrer equation on a broadened peak at high angle suggests that KCC-1 is composed of grain particles with a diameter of around 12 Å. Having calculated the d spacing of KCC-1, ca. 3.97 Å, we postulated the presence of four medium-range ordered (MRO) planes. This explains that KCC-1 possesses a slightly ordered structure as well as other amorphous silica materials.[34,35] N_2 adsorption−desorption isotherms of synthesized KCC-1 are provided in Figure S3. The comparison of BET surface areas and pore volumes is tabulated in the Supporting Information (Table S-1). According to the isotherm of KCC-1 in some previous reports,[10,12,14,15,19,20] KCC-1 has a type IV isotherm with H1 or H3 hysteresis loops. Most reports showed H3 hysteresis loops that are given by nonrigid aggregates of plate-like particles,[36] which supported our new classification criteria in which KCC-1 has lamellar morphology. These are in good agreement with our synthesized KCC-1 samples that also show the same type of isotherm and similar hysteresis loops.

Analysis of KCC-1 Emulsion. It has been said that the formation of KCC-1 involves the microemulsion system.[9,11,12,37] However, no experimental evidence has been reported concerning the transparency and stability of the microemulsion.[38] Here, we have conducted a Tyndal experiment to examine the scattering effect of the KCC-1 colloidal mixture when it is illuminated by a narrow beam of light. A green laser pointer was used to demonstrate the Tyndall effect on each precursor mixture of KCC-1. We have tested a precursor mixture in an aqueous phase containing CTAB, urea, and water as well as a precursor mixture in an organic phase containing toluene, butanol, and TEOS. The Tyndall effect was observed for both solutions in which the green light shone through the solution (Supporting Information, Figure S4a-b). The KCC-1 colloidal mixture was prepared by mixing the solution in the aqueous phase with solution in the organic phase. It was observed that the green laser did not pass through the mixture during the Tyndall experiment (Figure S4c). This suggests that the KCC-1 mixture contains large particles of more than 1 μm in diameter. This size is obtained from the DLS measurement. After 20 h, this milky mixture is unstable and separates into two phases (Figure S4c). It seems that the KCC-1 colloidal mixture does not have the properties of a microemulsion. This mixture, in fact, shows the existence of a macroemulsion that is thermodynamically unstable (droplet size of around 1−10 μm)[39−43] or the existence of a miniemulsion with 50 to 500 nm droplets.[44] Thus, the KCC-1 colloidal mixture is considered to be a macroemulsion.

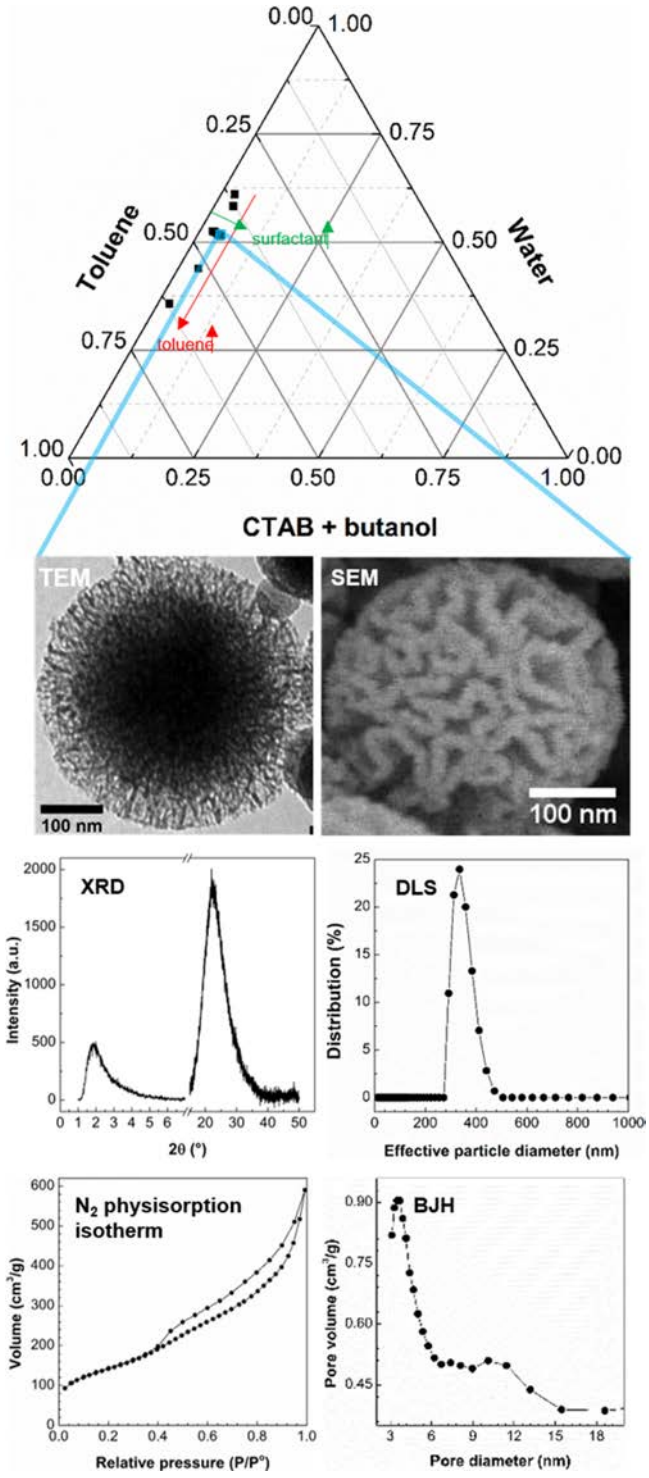

Figure 4. Ternary phase diagram of precursor composition to synthesize KCC-1 showing bicontinuous concentric lamellar morphology. The TEM image, SEM image, XRD diffractograms, DLS particle size distribution, N_2 physisorption isotherm, and BJH pore size distribution of synthesized KCC-1 on selected point in the diagram are shown here. Detailed SEM images of other samples are provided in Supporting Information (Figures S-1 and S-2).

The cmc value of the KCC-1 mother emulsion was determined by correlating specific conductivity (κ) with various surfactant concentrations (Figure 5). The plot shows that the higher the concentration of CTAB, the higher the conductivity. Moreover, an increase in the electrical conductivity was observed

DOI: 10.1021/acs.langmuir.6b00675
Langmuir 2016, 32, 5802−5811

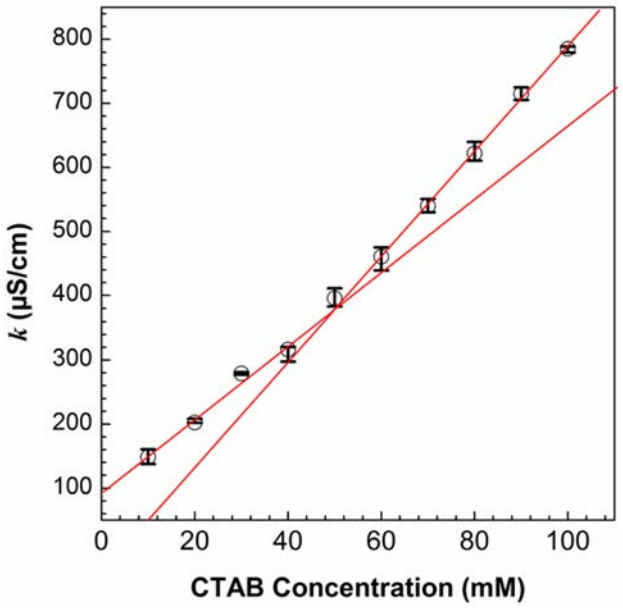

Figure 5. Dependence of specific conductivity on CTAB concentration for the CTAB/H_2O/toluene/butanol system.

as the CTAB concentration increased. This type of electrical conductivity dependence on the surfactant concentration is well known as the physical properties of reverse micellar systems.[45,46] As the CTAB concentration increases, the CTAB molecules tend to aggregate and form either normal micelles or reverse micelles. As is known, the electrical conductivity of such systems is very sensitive to their microstructure. In a normal micelle system, the conductivity of the ionic surfactant solution decreases at the CMC. However, a recent study confirmed that the normal micelles make no contributions to the conductivity as carriers of electric current, as discussed briefly in another report.[47] The conductivity is solely due to the small ions, i.e., the free counterions, the surfactant monomers, and the ions of added salts. The reason for such a decrease is considered to be due to the close packing of charged particles (including micelles) that suppress the micelle mobility. Whereas the study of reverse micellar systems has been widely focused on in percolation phenomena, which are characterized by remarkable increases in electrical conductivity when the water volume fraction or the temperature reaches a certain threshold value. It is generally considered that this phenomenon may occur as a result of static or dynamic droplet fusion.[48−51] However, at low volume fractions, another increase in conductivity has already been reported, and this increase was attributed to a change in the structure of the emulsion that occurs as one approaches the cmc of the surfactant.[46,50] Thus, the cmc can be evaluated from the deflection point of a plot of the electrical conductance against the surfactant concentration.[45] The deflection point was determined from the intersection of the two fitted lines of the experimental data, and the values on the x axis taken as the cmc values are in the concentration range of 48−53 mM. These values correspond to the cmc of CTAB reverse micelles.[45,52] The increase in CTAB concentration marks the formation of reverse micelles and supports larger amounts of water dissolved inside the core. Previous reports on the cmc of CTAB reverse micelles in chloroform and water are in agreement with this measurement, showing a value of 43 mM. Unlike the KCC-1 emulsion, the conductivity of aqueous CTAB solution increases with increasing CTAB concentration, and no further significant increase after a certain concentration indicates the onset of normal micelle formation.[53] This saturation implies an effective loss of ionic charge caused by the confinement effect of counterions ion the micellar surface. We found that the CTAB concentration used in the synthesis of KCC-1 in the previous reports and our study were slightly below the cmc value of CTAB reverse micelle. This value has been verified, and it is propotional to the square root of the concentration of undissociated surfactant found in the literature.[54]

In the reported and present study of KCC-1, the CTAB concentration was slightly below the cmc value of CTAB reverse micelles. In other words, the CTAB concentration of KCC-1 emulsion is much higher than the cmc value of a normal CTAB micellar solution. This might lead to an understanding that the micelles formed in the mixture of precursors affects the KCC-1 emulsion. To discuss the possible role of micelles in the formation of KCC-1, Raman spectra of the KCC-1 emulsion were compared to those of the CTAB micellar solution and pure water (Figure 6).

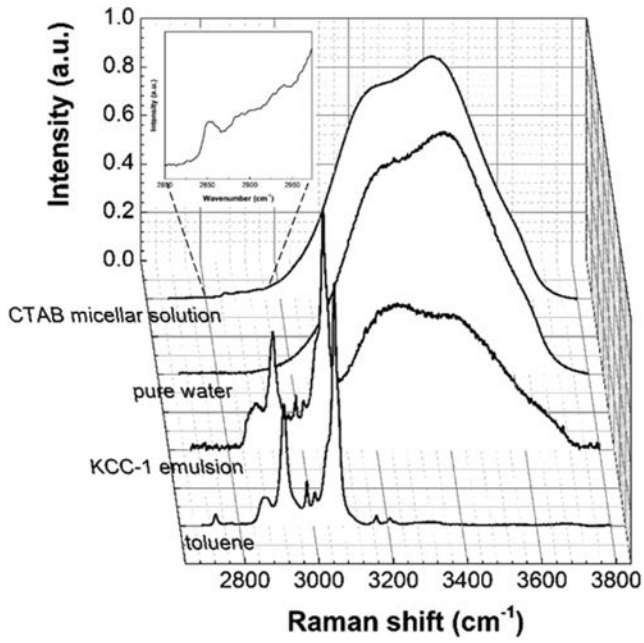

Figure 6. Raman spectra of CTAB in water (micellar solution), pure water, the KCC-1 emulsion, and toluene. The inset shows three distinguished peaks in the CTAB micellar solution.

Essentially, the Raman spectrum of the KCC-1 emulsion was identified to have major vibrational bands, i.e., a toluene band (2700−3100 cm^{-1})[55] and a water band (2800−3800 cm^{-1}).[56−60] The toluene band was verified after having compared with the Raman spectrum of toluene on a qualitative basis. The profile of the water band of the KCC-1 emulsion appears to be different from either the water band of the micellar solution or pure water. Meanwhile, the Raman spectra of the CTAB micellar solution and pure water look identical. From the water band, the local H-bonded network can be classified as to whether it is a proton donor (D), a proton acceptor (A), or a combination of both neighboring molecules.[56] To elucidate the differences, the Raman OH stretching bands of pure water and the KCC-1 emulsion were deconvoluted (Figure 7). The deconvoluted bands for both spectra resulted in vibrational peaks associated with $\nu_{DAA\text{-}OH}$, $\nu_{DDAA\text{-}OH}$, $\nu_{DA\text{-}OH}$, $\nu_{DDA\text{-}OH}$, and free OH symmetric

DOI: 10.1021/acs.langmuir.6b00675
Langmuir 2016, 32, 5802−5811

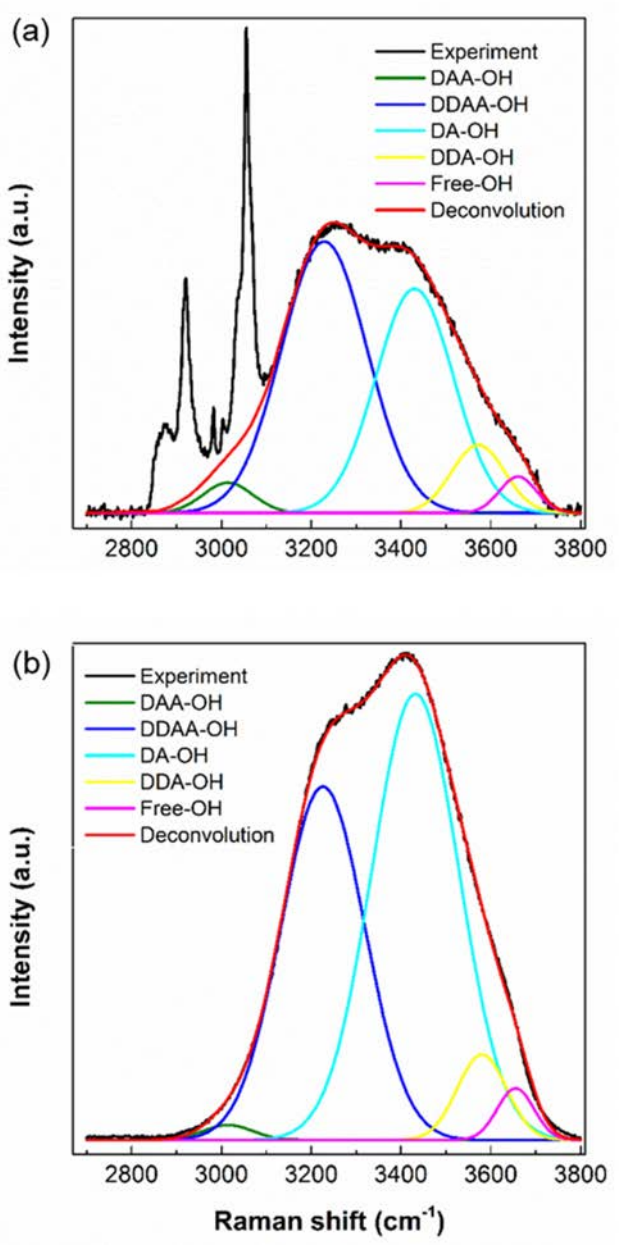

Figure 7. Raman spectral band deconvolution of OH stretching of (a) KCC-1 emulsion and (b) pure water.

Table 1. Frequency of OH Stretching Subbands of Raman Spectra of Water and the KCC-1 Emulsion

	frequency (cm^{-1})	
mode	pure water	KCC-1 emulsion
DAA-OH	3014	3014
DDAA-OH	3226	3229
DA-OH	3432	3430
DDA-OH	3580	3572
free-OH	3655	3660

stretching vibrations.[56] The detailed peak assignments are tabulated in Table 1. DDAA-OH (tetrahedral) and DA-OH (ring or chain) are the predominant H-bondings among the five deconvoluted bands. It is observed that in the KCC-1 emulsion, DDAA-OH exhibits a higher intensity than does DA-OH (Figure 7a). This phenomenon also reflects the Raman spectrum of ice crystals where the increase in tetrahedral H-bonding indicates a more bonded water molecule.[58,60−62] This condition also can be found in the confined water system, such as in reverse micelles and living plant cells. In principle, a living plant cell is a naturally confined liquid water system, and its OH stretching band is similar to that in the KCC-1 emulsion. In a reverse micelle system, water molecules are confined to the center of a micelle, and this leads to a more isolated water environment. The milieu is, then, good for driving full hydrogen bonding in the neighboring molecules, just as in the ice crystals.[56,62] These properties are in contrast to those of DDAA-OH and DA-OH in pure water (Figure 7b), which are identical in intensity to the OH stretching subbands with respect to those in the CTAB micellar solution.

The CTAB micellar solution shows small bands associated with the C−H Raman stretching vibration (inset of Figure 6). The peaks at 2850, 2880, and 2930 cm^{-1} can be distinguished as fingerprints of the CTAB micelle. This CTAB band, in principle, should also be present in the Raman spectrum of the KCC-1 emulsion because the CTAB concentration in the emulsion is far above the cmc value of normal micelles. However, the intense toluene band might overlap with the CTAB micelle fingerprint, which has low-intensity peaks. These might be responsible for the disappearance of the CTAB fingerprint in the KCC-1 Raman spectrum.

From Table 1, we can see that there are changes in several mode frequencies in pure water compared to those of the KCC-1 emulsion. By considering our Raman spectral resolution, when the change in these frequencies is more than 2 cm^{-1}, then the mode is shifted. Fully bonded and fully free-OH stretching subbands (DDAA-OH and free-OH, respectively) have higher frequencies in the KCC-1 emulsion compared to those in pure water. This means that both of the sub-bands experienced hardening. This can be attributed to a more confined environment in the KCC-1 emulsion. However, this is in contrast to three-bond subband such as DDA-OH and DAA-OH. Even DDA-OH was observed to be softened. This phenomenon may be explained by the capability of water molecules to have (up to) four local hydrogen-bonding networks. In DDA-OH mode, there is one free network in the water molecule. This condition may increase the probability of the molecule in making three hydrogen bonds with neighboring molecules.

Formation Mechanism of KCC-1. The formation of KCC-1 is drawn after the disclosure of several physical characteristics starting from the emulsion properties to the local structure of water molecules in the KCC-1 emulsion. The evidence of reverse micelle formation and the kinetic study of KCC-1 synthesis along with the observation of a morphological evolution further completes the portrait of KCC-1 formation and the determination of a definite type of forming morphology. It is interesting that the alcohol, e.g., *n*-butanol, has to cooperate hand-in-hand with CTAB at the micellar interface in the formation of reverse micelles[63] in the KCC-1 colloidal mixture. Otherwise, alcohol forms complexes with free CTAB molecules in solution and hinders reverse micelle formation. When reverse micelles occurs, two scenarios can be postulated: (i) Butanol is located in the micellar interface water pools.[63,64] At low CTAB concentration, this alcohol interacts only with water, but at high CTAB concentration, it also forms a complex with CTAB molecules at the micellar interface. (ii) CTAB molecules withdraw from the micelles and form complexes with alcohols and subsequently with other molecules in the bulk of the solution. On the other hand, alcohol molecules also

DOI: 10.1021/acs.langmuir.6b00675
Langmuir 2016, 32, 5802−5811

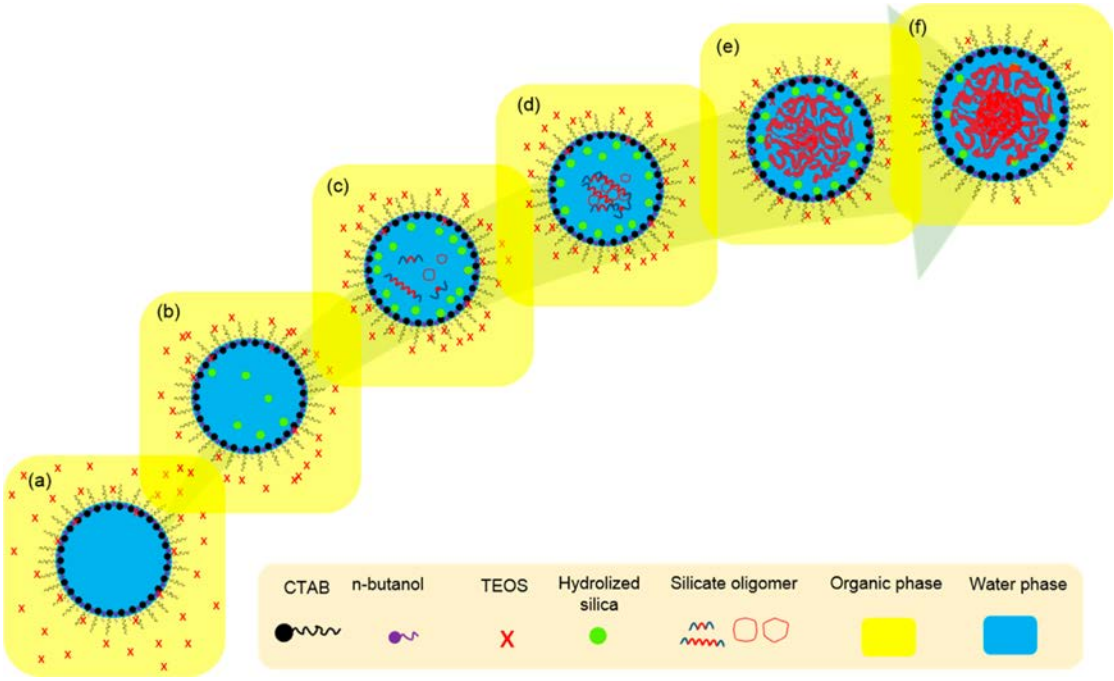

Figure 8. Schematic representation of the proposed formation mechanism of KCC-1: (a) TEOS diffusion into a phase boundary, (b) TEOS hydrolysis, (c) silica condensation, (d) silicate oligomers gathered around and followed by the phase segregation of condensation and hydrolysis products, (e) formation of a bicontinuous structure, and (f) development of bicontinuous concentric morphology.

penetrate the micelles to form complexes with CTAB in the interface.

Cationic reverse micelles that formed when cations were used dissolve less water than most anionic reverse micelles. It is reported that alcohol can decrease the surface tension of a water/organic system and aid the formation of an emulsion with good stability. It has a stabilizing effect on the interfacial layer, which results in a widening of the emulsion area. Therefore, it is believed that the alcohol is integrated into the interfacial layer of the emulsion droplet. Water droplets can be protected quickly by CTAB, and the layer between two colliding water droplets becomes stable. This seems to stabilize the emulsion, which is thermodynamically unstable before the condensation of silica takes place.

Figure 8 illustrates a plausible formation mechanism of KCC-1. To describe these elementary processes after the generation of reverse micelles, some aspects that stimulate the formation of a silica network are explained. The first aspect is the hydrophobic interaction between silica precursor (TEOS) molecules and the hydrophobic tail of CTAB. Another aspect would be the concentration gradient of TEOS inside and outside the reverse micelles, which creates a high chemical potential. These two aspects drive the molecules of TEOS in the organic phase to diffuse and approach the tail of CTAB. Herein, TEOS molecules may interact with the tail and reach the phase boundary of reverse micelle (Figure 8a). Once the molecules reach the boundary and make contact with water at the phase boundary of the micelle, the hydrolysis reaction occurs, yielding ethanol and silanol groups. All products from this hydrolysis then penetrate the reverse micelle as a result of their polarity (Figure 8b).

Prior to solvothermal treatment, the pH of the KCC-1 emulsion was measured before and after 30 min of stirring applied to the emulsion. The pH decreased from 8.14 to 6.89. This means that the hydrolysis of TEOS and the condensation of silica occur under basic conditions. The hydrolysis reaction is then followed by a condensation reaction producing water and siloxane. Silica condensation under basic conditions is preferably at the internal Si atoms' position to produce a branched silica polymer (polysiloxane)[65] (Figure 8c). However, the formation of siloxy groups will induce water protonation, which slows hydrolysis, and further protonation lowers the pH and decelerates the formation of further branched silica oligomers. Meanwhile, linear silica oligomers tend to form a closed structure.[66−69] For instance, a three-ring structure is easily formed, but it is also easy for a three-ring structure to reopen and form a linear trimer. When the pH is around 8, the formation of the four-ring structure is the most rapid, indicating faster particle growth. These rings contribute to the hydrophobic property of the formed silica oligomer structure. Then, further hydrolysis, condensation, and siloxy group formation decrease the pH and hinder ring formation at pH 7.[68] This inhibition leads to the growth of linear oligomers, chiefly tetramers.[68] Eventually, the silica polymer tends to form a bicontinuous structure (Figure 8d−f).

The generation of a bicontinuous structure during KCC-1 synthesis needs further explanation. We have conducted a kinetic study of KCC-1 synthesis via solvothermal treatment, hence observing the morphological evolution during solvothermal processes. TEM images show that the morphology of KCC-1 developed from a small spherical bicontinuous structure into a larger one (Figure 9).

The enhancement of the KCC-1 particle can be explained on the basis of ABA triblock copolymer self-assembly. However, during the condensation reaction, the chain length of polysiloxane cannot be experimentally verified as to whether it has a similar repeating unit of the Si−O−Si chain. The decreasing pH during polysiloxane chain growth leads to the formation of polysiloxane with various lengths of the Si−O−Si chain. On the basis of their structures, there are some polar

DOI: 10.1021/acs.langmuir.6b00675
Langmuir 2016, 32, 5802−5811

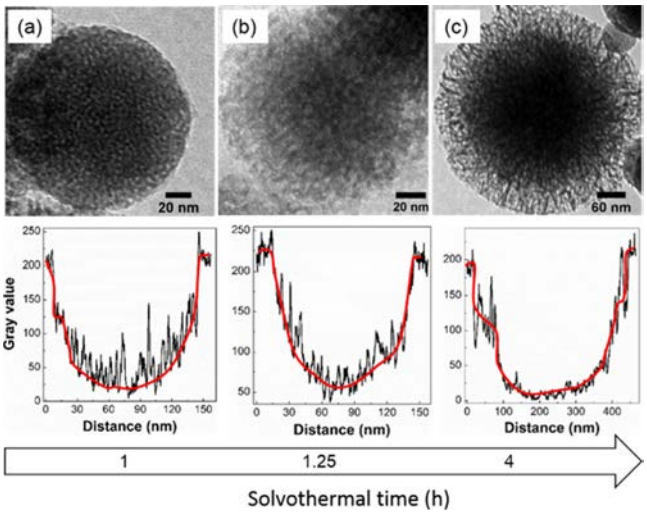

Figure 9. TEM images resulting after kinetically studying the synthesis of KCC-1. The bicontinuous concentric lamellar morphology was observed from (a) a nonconcentric condition, (b) a concentric condition, and (c) a more concentric condition. The TEM profiles of each image are shown below.

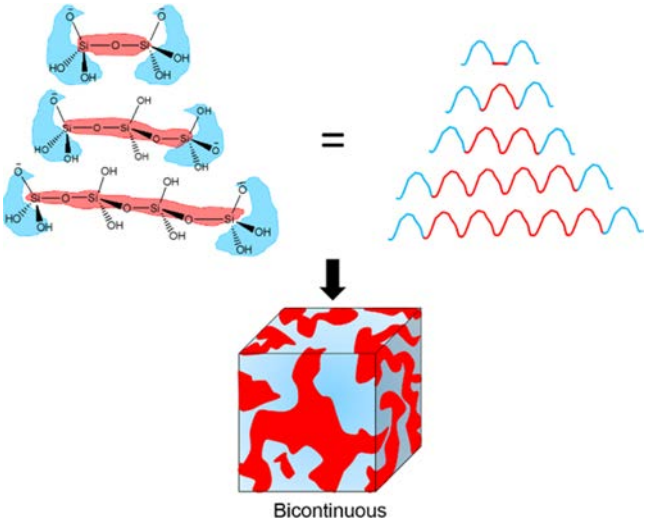

Figure 10. Self-assembly of the silicate oligomer. The ABA silicate oligomer consists of two A blocks (blue) separated by a B block (red), where the A block consists of O−H groups in the terminal and the B block is the Si−O−Si chain of the oligomers. This pattern is similar to ABA triblock copolymer chains where A and B blocks are formed from different monomers. When B blocks of the polysiloxane have a range of chain lengths, a bicontinuous structure is formed (redrawn from ref 71).

hydroxyl groups (A) at the end of polysiloxane and a nonpolar Si−O−Si chain (B) (Figure 10). The longer the Si−O−Si chain, the more hydrophobic the polymer. In silicate compounds, both of these domains compose with an ABA pattern. In other words, the polysiloxane structure can be regarded as a polymer with ABA structure as well as a triblock copolymer. In a self-assembling polymer, it is well known[69,70] that molecules of ABA triblock copolymers (in which A and B represent different blocks) robustly generate an unusually stable bicontinuous structure containing separate A and B domains when the middle blocks have a broad range of length. That structure confirms that neither a narrow distribution nor a particularly high molar mass is required to make bicontinuous structures. Nevertheless, all that seems necessary is that the polydisperse B blocks should be tethered at a minimum of two points.[71] Here, we presume that the irregularity in the polysiloxane Si−O−Si chain length may lead to the formation of bicontinuous morphology.

This bicontinuous structure may also be produced from the phase segregration process of the polymers. As a consequence of hydrolysis and the condensation reaction, hydrophobic molecules (polysiloxane) and hydrophilic molecules (water and ethanol) are produced in the core of reverse micelle. This situation may trigger phase segregation between hydrophobic and hydrophilic sections as a result of excessive polysiloxane, silica rings, ethanol, and water molecules (Figure 8d). The increase in water content may enhance the size of reverse micelles.

The silica structure is getting denser as observed in the TEM images of products by prolonging the solvothermal treatment. Further condensation reactions may lead to the formation of a denser silica structure resulting from the cross-linking process (Figure 9f). TEM and FE-SEM images (Figure S5) show a cross section of synthesized KCC-1. It can be seen that the density of KCC-1 particles decreases inside out. This indicates that silica condensation in the micelle is more intense in the middle part. This may be caused by surfactant polar headgroups in the shell of reverse micelle that attract another polar molecule such as water and ethanol. It is known that the presence of ethanol molecules can retard the hydrolysis process and that excess water slows the condensation process in the outer part. Thus, silica condensation in the outer part is slower than in the inner part. The inner part of the micelle is also a better place for silica networking. Therefore, the silica formed a denser structure that was observed as a concentric pattern.

CONCLUSIONS

By quantitatively analyzing the TEM images, we can differentiate KCC-1 from other spherical particles with similar morphologies. The interpretation of morphology both from the SEM image and the TEM profile led to a more representative term called bicontinuous concentric lamellar. The formation of KCC-1 is initiated by the formation of reverse micelle in the mixture of starting material, followed by the hydrolysis of TEOS molecules at the interface and penetration of the products in the aqueous phase of reverse micelles. The condensation process occurred in a polydisperse manner, giving Si−O−Si repeating units of various lengths. The next step is the phase segregation of hydrophobic and hydrophilic sections because polysiloxane, silica ring, ethanol, and water molecules stampede inside the reverse micelle. Further condensation led to cross-linking process. These processes stimulate the growth of the reverse micelle size. The condensation also produces water and ethanol that tend to interact with the CTAB polar head in the micelle exterior. This condition hampered condensation in the outer part, causing more rapid condensation in the micelle inner part. Therefore, KCC-1 particles with a denser structure in the middle are formed and indeed observed by TEM as a concentric pattern.

ASSOCIATED CONTENT

Supporting Information

The Supporting Information is available free of charge on the ACS Publications website at DOI: 10.1021/acs.langmuir.6b00675.

Ternary phase diagram, SEM analysis, N_2 physisorption, and Tyndall effect analysis results (PDF)

DOI: 10.1021/acs.langmuir.6b00675
Langmuir 2016, 32, 5802−5811

AUTHOR INFORMATION

Corresponding Authors

*Tel: +62-22-250-2103. Fax: +62-22-250-4154. E-mail: vsuendo@chem.itb.ac.id.

*Tel: +62-22-250-2103. Fax: +62-22-250-4154. E-mail: rino@chem.itb.ac.id.

Author Contributions

All authors have given approval to the final version of the manuscript.

Funding

This work was supported in part by The Asahi Glass Foundation, SINas, and Hibah PMDSU Phase I research grants.

Notes

The authors declare no competing financial interest.

ACKNOWLEDGMENTS

E.F. thanks The Ministry of Research, Technology, and Higher Education (Menristekdikti) of Indonesia for the PMDSU scholarship program.

REFERENCES

(1) Munnik, P.; de Jongh, P. E.; de Jong, K. P. Recent Developments in the Synthesis of Supported Catalysts. *Chem. Rev.* **2015**, *115*, 6687−6718.

(2) Serrano, D. P.; Escola, J. M.; Pizarro, P. *Chem. Soc. Rev.* **2013**, *42*, 4004−4035.

(3) Chaikittisilp, W.; Muraoka, K.; Ji, W.; Ariga, K.; Yamauchi, Y. *J. Mater. Chem. A* **2014**, *2*, 12096−12103.

(4) Weidmann, C.; Brezesinski, K.; Suchomski, C.; Tropp, K.; Grosser, N.; Haetge, J.; Smarsly, B. M.; Brezesinski, T. Morphology-Controlled Synthesis of Nanocrystalline η-Al_2O_3 Thin Films, Powders, Microdbeads, and Nanofibers with Tunable Pore Sizes from Preformed Pligomeric Oxo-Hydroxo Building Blocks. *Chem. Mater.* **2012**, *24*, 486−494.

(5) Yanagisawa, T.; Shimizu, T.; Kuroda, K.; Kato, C. The Preparation of Alkyltrimethylammonium-kanemite Complexes and Their Conversion to Microporous Material. *Bull. Chem. Soc. Jpn.* **1990**, *63*, 988−992.

(6) Kresge, C. T.; Leonowicz, M. E.; Roth, W. J.; Vartuli, J. C.; Beck, J. S. Ordered Mesoporous Molecular Sieves Synthesized by A Liquid-crystal Template Mechanism. *Nature* **1992**, *359*, 710−712.

(7) Zhao, D. Y.; Feng, J.; Huo, Q.; Melosh, N.; Fredrickson, G. H.; Chmelka, B. F.; Stucky, G. D. Triblock Copolymer Syntheses of Mesoporous Silica with Periodic 50 to 300 Angstrom Pores. *Science* **1998**, *279*, 548−552.

(8) Che, S.; Liu, Z.; Ohsuna, T.; Sakamoto, K.; Terasaki, O.; Tatsumi, T. Synthesis and Characterization of Chiral Mesoporous Silica. *Nature* **2004**, *429*, 281−284.

(9) Polshettiwar, V.; Cha, D.; Zhang, X.; Basset, J. M. High-Surface-Area Silica Nanospheres (KCC-1) with a Fibrous Morphology. *Angew. Chem., Int. Ed.* **2010**, *49*, 9652−9656.

(10) Polshettiwar, V.; Basset, J. M. High surface area fibrous silica nanoparticles. U.S. Patent 2011/0253643 A1, October 20, 2011.

(11) Fihri, A.; Bouhrara, M.; Patil, U.; Cha, D.; Saih, Y.; Polshettiwar, V. Fibrous Nano-Silica Supported Ruthenium (KCC-1/Ru): A Sustainable Catalyst for the Hydrogenolysis of Alkanes with Good Catalytic Activity and Lifetime. *ACS Catal.* **2012**, *2*, 1425−1431.

(12) Bouhrara, M.; Ranga, C.; Fihri, A.; Shaikh, R. R.; Sarawade, P.; Emwas, A. H.; Hedhili, M. N.; Polshettiwar, V. Nitridated Fibrous Silica (KCC-1) as a Sustainable Solid Base Nanocatalyst. *ACS Sustainable Chem. Eng.* **2013**, *1*, 1192−1199.

(13) Thankamony, A. S. L.; Lion, C.; Pourpoint, F.; singh, B.; Linde, A. j. P.; Carnevale, D.; Bodenhausen, G.; Vezin, H.; Lafon, O.; Polshettiwar, V. Insights into the Catalytic Activity of Nitridated Fibrous Silica (KCC-1) Nanocatalysts from 15N and 29Si NMR Spectroscopy Enhanced by Dynamic Nuclear Polarization. *Angew. Chem., Int. Ed.* **2015**, *53*, 1−5.

(14) Dhiman, M.; Chalke, B.; Polshettiwar, V. Efficient Synthesis of Monodisperse Metal (Rh, Ru, Pd) Nanoparticles Supported on Fibrous Nanosilica (KCC-1) for Catalysis. *ACS Sustainable Chem. Eng.* **2015**, *3*, 3224−3230.

(15) Singh, B.; Polshettiwar, V. Design of CO_2 sorbents using functionalized fibrous nanosilica (KCC-1): insights into the effect of the silica morphology (KCC-1 vs. MCM-41). *J. Mater. Chem. A* **2016**, DOI: 10.1039/C6TA01348A.

(16) Yang, P.; Gai, S.; Lin, J. Functionalized Mesoporous Silica Materials for Controlled Drug Delivery. *Chem. Soc. Rev.* **2012**, *41*, 3679−3698.

(17) Wan, Y.; Zhao, D. On the Controllable Soft-Templating Approach to Mesoporous Silicates. *Chem. Rev.* **2007**, *107*, 2821−2860.

(18) Barton, T. J.; Bull, L. M.; Klemperer, W. G.; Loy, D. A.; McEnaney, B.; Misono, M.; Monson, P. A.; Pez, G.; Scherer, G. W.; Vartuli, J. C.; Yaghi, O. M. Tailored Porous Material. *Chem. Mater.* **1999**, *11*, 2633−2656.

(19) Gai, S.; Yang, P.; Ma, P.; Wang, L.; Li, C.; Zhang, M.; Jun, L. Uniform and Size-Tunable Mesoporous Silica with Fibrous Morphology for Drug Delivery. *Dalton Trans.* **2012**, *41*, 4511−4516.

(20) Moon, D. S.; Lee, J. K. Tunable Synthesis of Hierarchical mesoporous Silica Nanoparticles with Radial Wrinkle Structure. *Langmuir* **2012**, *28*, 12341−12347.

(21) Du, X.; Qiao, S. Z. Dendritic Silica Particles with Center-Radial Pore Channels: Promising Platforms for Catalysis and Biomedical Applications. *Small* **2015**, *11*, 392−413.

(22) Guo, Q.; Singh, V.; Behrens, S. H. Electric Charging in Nonpolar Liquids Because of Nonionizable Surfactants. *Langmuir* **2010**, *26*, 3203−3207.

(23) Schneider, C. A.; Rasband, W. S.; Eliceiri, K. W. NIH Image to ImageJ: 25 Years of Image Analysis. *Nat. Methods* **2012**, *9*, 671−675.

(24) Collins, T. J. ImageJ for Microscopy. *BioTechniques* **2007**, *43*, S25−S30.

(25) Dong, Q.; Dong, A.; Morigen. Evaluation of Novel Antibacterial *N*-Halamine Nanoparticles Prodrugs towards Susceptibility of *Escherichia coli* Induced by DksA Protein. *Molecules* **2015**, *20*, 7292−7308.

(26) Hah, H. J.; Kim, J. S.; Jeon, B. J.; Koo, S. M.; Lee, Y. E. Simple Preparation of Monodisperse Hollow Silica Particles without using Templates. *Chem. Commun.* **2003**, 1712−1713.

(27) Pauwels, B.; van Tendeloo, G.; Thoelen, C.; van Rhijn, W.; Jacobs, P. A. Structure Determination of Spherical MCM-41 Particles. *Adv. Mater.* **2001**, *13*, 1317−1320.

(28) Liu, J.; Hartono, S. B.; Jin, Y. G.; Lu, G. Q.; Qiao, S. Z. A Facile Vesicle Template Route to multi-Shelled Mesoporous Silica Hollow Nanospheres. *J. Mater. Chem.* **2010**, *20*, 4595−4601.

(29) Chen, D.; Li, L. L.; Tang, F. Q.; Qi, S. Facile and Scalable synthesis of Tailored Silica "Nanorattle" Structures. *Adv. Mater.* **2009**, *21*, 3804−3807.

(30) Fang, B.; Kim, J. H.; Kim, M. S.; Yu, J. S. Hierarchical Nanostructured Carbons with meso-Macroporosity: Design, Characterization, and Applications. *Acc. Chem. Res.* **2013**, *46*, 1397−1406.

(31) Gao, D.; Zhang, Z.; Wu, M.; Xie, C.; Guan, G.; Wang, D. A Surface Functional Monomer-Directing Strategy for Highly Dense Imprinting of TNT at Surface of Silica Nanoparticles. *J. Am. Chem. Soc.* **2007**, *129*, 7859−7866.

(32) Yang, H.; Liao, S.; Huang, C.; Du, L.; Chen, P.; Huang, P.; Fu, Z.; Li, Y. Facile One-Pot Approach to the Synthesis of Spherical Mesoporous Silica Nanoflowers with Hierarchical Pore Structure. *Appl. Surf. Sci.* **2014**, *314*, 7−14.

(33) Mukti, R. R.; Hirahara, H.; Sugawara, A.; Shimojima, A.; Okubo, T. Drect Hydrothermal Synthesis of Hierarchically Porous Siliceous Zeolite by Using Alkoxysilylated Nonionic Surfactant. *Langmuir* **2010**, *26*, 2731−2735.

(34) Manaila, R.; Zaharescu, M. Local Order in High Surface Area Amorphous Silica. *Phys. Status Solidi* **1986**, *98*, 377−382.

DOI: 10.1021/acs.langmuir.6b00675
Langmuir 2016, 32, 5802−5811

(35) Pophal, C.; Fuess, H. Investigation of the medium Range Order of Polyhedra Forming the Walls of MCM-41 − An X-ray Diffraction Study. *Microporous Mesoporous Mater.* **1999**, *33*, 241−247.
(36) Thommes, M.; Kaneko, K.; Neimark, A. V.; Olivier, J. P.; Reinoso, F. R.; Rouquerol, J.; Sing, K. S. W. Physisorption of Gases, with Special Reference to the Evaluation of Surface Area and Pore Size Distribution (IUPAC Technical Report). *Pure Appl. Chem.* **2015**, *87*, 1051−1069.
(37) Wang, L.; Imura, M.; Yamauchi, Y. Tailored Design of Architecturally Controlled Pt Nanoparticles with Huge Surface Areas toward Superior Unsupported pt Electrocatalysts. *ACS Appl. Mater. Interfaces* **2012**, *4*, 2865−2869.
(38) McClements, D. J. Nanoemulsions versus Microemulsions: Terminology, Differennces, and Similarities. *Soft Matter* **2012**, *8*, 1719−1729.
(39) Ouyang, Y.; Mansell, R. S.; Rhue, R. D. Flow of Gasoline-in-water Microemulsion Through Water-Saturated Soil Columns. *Groundwater* **1995**, *33*, 399−406.
(40) Kabalnov, A.; Wennerstrom, H. Macroemulsion Stability: The Oriented Wedge Theory Revisited. *Langmuir* **1996**, *12*, 276−292.
(41) Kabalnov, A.; Weers, J. Macroemulsion Stability within the Winsor III Region: Theory versus Exoeriment. *Langmuir* **1996**, *12*, 1931−1935.
(42) Chern, C. S.; Liu, C. W. Effect of Short-Chain Alcohols on the Oil-in-Water Microemulsion Polymerization of Styrene. *Colloid Polym. Sci.* **2000**, *278*, 329−336.
(43) Gupta, D. K.; Mohanty, K. K. A Laboratory Stdy of Surfactant Flushing of DNAPL in the Presence of Macroemulsion. *Environ. Sci. Technol.* **2001**, *35*, 2836−2843.
(44) Kawahara, H.; Goto, T.; Ohnishi, K.; Ogura, H.; Kage, H.; Matsuno, Y. Preparation of Epoxy Resin/Acrylic Composite Latexes by Miniemulsion Polymerization Method. *J. Appl. Polym. Sci.* **2001**, *81*, 128−133.
(45) Klicova, L.; Sebej, P.; Stacko, P.; Filippov, S. K.; Bogomolova, A.; Padilla, M.; Klan, P. CTAB/Water/Chloroform reverse Micelles: A Closed or Open Association Model. *Langmuir* **2012**, *28*, 15185−15192.
(46) Eicke, H. f.; Borkovec, M.; Gupta, B. D. Conductivity of Water-in-Oil Microemulsions: A Quantitative Charge Fluctuation Model. *J. Phys. Chem.* **1989**, *93*, 314−317.
(47) Danov, K. D.; Kralchevsky, P. A.; Ananthapadmanabhan, K. P. Micelle-Monomer Equilibria in Solutions of Ionic Surfactants and in Ionic-Nonionic Mixtures: A Generalized Phase Separation Model. *Adv. Colloid Interface Sci.* **2014**, *206*, 17−45.
(48) Paul, B. K.; Mitra, R. K. Conductivity of Reverse Micellar Systems of water/AOT + Brij-56 or Brij-58/IPM and Their Percolaton under Varied Concentrations of Amphiphiles and Different Additives. *Colloids Surf., A* **2006**, *273*, 129−140.
(49) Alexandridis, P.; Holzwarth, J. F.; Hatton, T. A. Thermodynamics of Droplet Clustering in Percolating AOT Water-in-Oil Microemulsions. *J. Phys. Chem.* **1995**, *99*, 8222−8232.
(50) Lagourette, B.; Peyrelasse, J.; Boned, C. Percolative Conduction in Microemulsion Type Systems. *Nature* **1979**, *281*, 60−62.
(51) Eicke, H. F.; Hammerich, H.; Vasta, G. A Thermodynamic Analysis of the Molar Conductivity of the ternary System: Water-Aerosol OT-isooctane. *J. Colloid Interface Sci.* **1983**, *93*, 593−595.
(52) Khan, A. M.; Shah, S. S. Determination of Critical Micelle (Cmc) of Sodium Dodecyl Sulfate (SDS) and the Effect of Low Concentration of Pyrene on Its SMC using Origin Software. *J. Chem. Soc. Pak.* **2008**, *30*, 186−191.
(53) Modaressi, A.; Sifaoui, H.; Grzesiak, B.; Solimando, R.; Domanska, U.; Rogalski, M. CTAB Aggregation in Aqueous Solutions of Ammonium based Ionic Liquids. *Colloids Surf., A* **2007**, *296*, 104−108.
(54) Sainis, S. K.; Merrill, J. W.; Dufresne, E. R. Electrostatic Interactions of Colloidal Particles at Vanishing Ionic Strength. *Langmuir* **2008**, *24*, 13334−13337.
(55) Bican, Th. S.; Schrotter, H. W.; Grosev, V. M. The Raman Spectrum of Toluene Vapour. *J. Raman Spectrosc.* **1995**, *26*, 787−790.
(56) Sun, Q. Local Statistic Interpretation for Water Structure. *Chem. Phys. Lett.* **2013**, *568*−*569*, 90−94.
(57) Sun, Q. The Raman OH Stretching Bands of Liquid Water. *Vib. Spectrosc.* **2009**, *51*, 213−217.
(58) Sun, Q.; Qin, C. Raman OH Stretching Band of Water as an Internal Standard to Determine Carbonate Concentrations. *Chem. Geol.* **2011**, *283*, 274−278.
(59) Sun, Q. Raman Spectroscopic Study of the Effects of Dissolved NaCl on Water Structure. *Vib. Spectrosc.* **2012**, *62*, 110−114.
(60) Sun, Q.; Zheng, H. Raman OH Stretching Vibration of Ice I_h. *Prog. Nat. Sci.* **2009**, *19*, 1651−1654.
(61) Salzmann, C.; Kohl, I.; Loerting, T.; Mayer, E.; Hallbrucker, A. Raman Spectroscopic Study on Hydrogen Bonding in Recovered Ice IV. *J. Phys. Chem. B* **2002**, *106*, 1−6.
(62) Cross, P. C.; Burnham, J.; Leighton, P. A. The Raman Spectrum and The Structure of Water. *J. Am. Chem. Soc.* **1937**, *59*, 1134−1137.
(63) Mathew, D. S.; Juang, R. S. Role of Alcohols in the Formation of Inverse Microemulsions and Back Extraction of Proteins/Enzymes in a Reverse Micellar System. *Sep. Purif. Technol.* **2007**, *53*, 199−215.
(64) Biais, J.; Bothorel, P.; Clin, B.; Lalanne, P. Phase Behaviour of Microemulsions Thermodynamics of the R-Theory. *J. Dispersion Sci. Technol.* **1981**, *2*, 67−95.
(65) Keefer, K. D. The Effect of Hydrolysis Condition on the Structure and Growth of Silicate Polymers. *MRS Online Proc. Libr.* **1984**, *32*, 15−24.
(66) Trinh, T. T.; Jansen, A. P. J.; van Santen, R. A. Mechanism of Oligomerization Reactions of Silica. *J. Phys. Chem. B* **2006**, *110*, 23099−23106.
(67) Trinh, T. T.; Jansen, A. P. J.; van Santen, R. A.; Meijer, E. J. The Role of Water in Silicate Oligomerization Reaction. *Phys. Chem. Chem. Phys.* **2009**, *11*, 5092−5099.
(68) Zhang, X. Q.; Trinh, T. T.; van Santen, R. A.; Jansen, A. P. J. Mechanism of the Initial Stage of Silicate Oligomerization. *J. Am. Chem. Soc.* **2011**, *133*, 6613−6625.
(69) Widin, J. M.; Schmitt, A. K.; Schmitt, A. L.; Im, K.; Mahanthappa, M. K. Unexpected Consequences of Block Polydispersity on the Self-Assembly of ABA Triblock Copolymers. *J. Am. Chem. Soc.* **2012**, *134*, 3834−3844.
(70) Widin, J. M.; Schmitt, A. K.; Im, K.; Schmitt, A. L.; Mahanthappa, M. K. Polydispersity-Induced Stabilization of Disordered Bicontinuous Morphology in ABA Triblock Copolymers. *Macromolecules* **2010**, *43*, 7913−7915.
(71) Register, R. A. Materials Science: Continuity Through Dispersity. *Nature* **2012**, *483*, 167−168.

DOI: 10.1021/acs.langmuir.6b00675
Langmuir 2016, 32, 5802−5811